


RESEARCH ARTICLE

Design and motion mechanism analysis of screw-driven in-pipe inspection robot based on novel adapting mechanism

Jihua Yin , Xuemei Liu, Youqiang Wang and Yucheng Wang

School of Mechanical & Automotive Engineering, Qingdao University of Technology, Qingdao, China
Corresponding author: Jihua Yin; Email: JihuaYin@outlook.com

Received: 11 April 2023; **Revised:** 8 January 2024; **Accepted:** 9 February 2024; **First published online:** 4 March 2024

Keywords: Screw-driven; in-pipe inspection robot (IPIR); pipe diameter adaption; motion mechanism

Abstract

In the pipeline industry, it is often necessary to monitor cracks and damage in pipelines, or need to clean the inside of the pipeline regularly, or collect adhesive on the inner wall of the pipe, but the pipe is too narrow and difficult for humans to enter, it is necessary to use a pipe machine to complete the work. In this paper, a newly designed screw-driven in-pipe inspection robot (IPIR) is proposed. Compared with common robots, this robot innovatively designs adapting mechanism. The robot can not only adapt to the change of the inner diameter size of the pipeline by using the bionic principle and the deformation characteristics of flexible components but also can pass smoothly in the horizontal/oblique/vertical pipelines and has a certain ability to cross obstacles. In addition, it can transmit images of the inner wall of the pipeline wirelessly for data analysis. Finally, through theoretical analysis and prototype construction, the performance of the robot is verified. The results show that the prototype robot can not only smoothly pass through the acrylic pipe with inner diameter of 120–138 mm but also pass through boss with a height of 3 mm.

1. Introduction

Pipelines are widely used as a means of transportation of nationally important materials such as solids, liquids, and gases. With the influence of heavy pressure, internal and external material corrosion, man-made damage, and geological layer movement, there are more and more hidden dangers in the pipeline, bringing many potential threats to people's life and property safety. Therefore, regular quality inspection and maintenance of the pipeline are necessary. Because the pipeline buried in the ground for a long time or placed in the outer wall of the building, it is difficult to detect and maintain by human. As a result, in order to replace human to complete inspection tasks [1], maintenance, and cleaning [2], among others robotics service, it is urgent to develop the pipeline robot.

At present, there are many researches on in-pipe robots. According to the movement mode of robots, they can be divided into wheel-driven robot, tracked/caterpillar type, walking/legged robot, inchworm type, PIG robot, and screw-driven type. Many researchers analyzed and summarized the characteristics of various types of robots [3–8]. Figure 1(a) shows a wheeled pipeline robot that relies on wheels to travel and cannot pass through steep or vertical pipes [9]. As shown in Fig. 1(b), the tracked pipeline robot changes the traditional wheel form into a track with stronger terrain adaptability. It can operate in harsh environment, but its size is too large to travel in the small-diameter pipeline [10]. The legged robot in Fig. 1(c) has strong adaptability to the pipeline structure, but the coordination of legs and feet is difficult to adjust and the motion control is complicated [11]. As depicted in Fig. 1(d), the inchworm-type robot mimics the movement mechanism of animal inchworm, which is stable in operation but slow in movement speed and low in working efficiency [12–14]. As shown in Fig. 1(e), PIG in-pipe

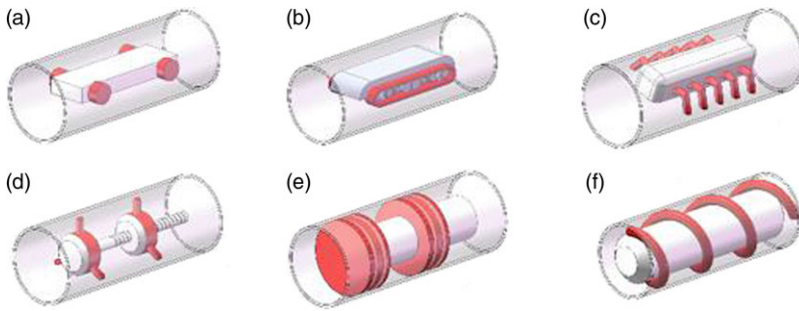


Figure 1. Types of in-pipe robots. (a) Wheel-driven robot, (b) tracked/caterpillar type, (c) walking/legged robot, (d) inchworm type, (e) PIG robot, (f) screw-driven type.

robot moves by the pressure difference of the medium in the pipeline, which affects the running speed [15]. Figure 1(f) shows the screw-driven robot spiraling forward along the inner wall of the pipeline. Although the motion efficiency is low, its motion control is simple and can adapt to vertical pipelines. Screw-driven robots have a large load capacity and can be used as modular extension design combination robots or equipped with robotic arms for pipeline operation tasks such as cleaning and repairing, with incomparable advantages. Therefore, the application prospects are very broad [16].

Regardless of the operating principle, robots need to have the ability to adapt to changes in pipeline diameter. Therefore, robots are usually designed with adapting mechanism to meet the needs of pipeline diameter changes. Table I compares and analyzes the adaptive mechanisms and advantages and disadvantages of the aforementioned five common robots (PIG robots are not analyzed due to the small application range of pipeline).

According to the reference, the wheel-driven robot adopts a car bottom plate design, without considering changes in pipeline diameter, and has low adaptability to pipeline working conditions. Other robots use a wall-pressed structure to travel along the inner wall of the pipeline. However, commonly wall-pressed structure robots have a single adaptive mechanism, which uses simple linkages, linkage combinations, slider-crank, etc., and this deformation mechanism can only be used for tracked, legged, and inchworm robots [26]. For screw-driven robots, the walking mechanism is composed of inclined driven wheels and guide wheels, and the diameter of the robot is passively adjusted through extension and contraction of the spring support arm. The mechanical structure is not very different, and innovative designs are urgently needed.

Up to now, there are many research directions for screw-driven pipeline robots, such as modular design [27, 28], efficiency optimization [29, 30], special pipeline travel [31, 32], etc. The adaptability and travel of robots to pipelines are the most basic performance. Based on the above analysis, most of the existing pipe robots are based on rigid frameworks, which have advantages for multi-degrees-of-freedom motion and precise control. However, their usually cumbersome bodies might be a limitation. With the rapid development of bionic robot research [33–37], it is easier to design robots with deformability and compatibility. A new design scheme for a spiral-driven pipeline inspection robot is proposed based on the bionic principle of flexible shaft deformation and combined with the principle of screw drive, breaking through the conventional linkage deformation mechanism and travel mechanism.

2. Proposed IPIR model

2.1. Proposed screw-driven IPIR

The design of the in-pipe robot needs to comprehensively consider the characteristics of the pipeline. The analysis of pipeline characteristics and robot requirements includes:

Table I. Comparison between the adapting mechanisms of the robots.

Types	Ref. No.	Adapting Mechanism	Diameter Range(mm)	Working conditions	Advantage	Disadvantage
Wheel	[17]	No	300	Horizontal pipes	Simple mechanism	Unable on pipe adjustment
Tracked/ Caterpillar	[18]	Linkage structure	300–450	Horizontal/Sloping pipes	High traction/ Stable and secure platform	More complicated mechanical structure/ Larger axial dimension
	[19]	Parallelogram mechanism with ball screw	813–1219	Curved pipes		
Walking/ Legged	[20]	Slider-crank mechanism	270–380	Horizontal/Sloping pipes	Able to pipe adjustment/ Stable and secure platform	Larger axial dimension/ Limited ability to carry heavy loads
	[21]	Slider-crank mechanism	130–180	Horizontal/Vertical/Elbow pipes		
Inchworm	[22]	Slider-crank mechanism	205–305	Horizontal/Vertical/Elbow pipes	Can through special pipelines	Interconnected modules with large size /Low motion speed
	[23]	Spring support leg	360–400	Horizontal pipes/U groove		
Screw-driven	[24]	No	200	Vertical curved pipes	High traction and steer-ability/ High control on speed	Unable to move in non-circular pipe
	[25]	Spring support arm	122–131	Curved pipes		

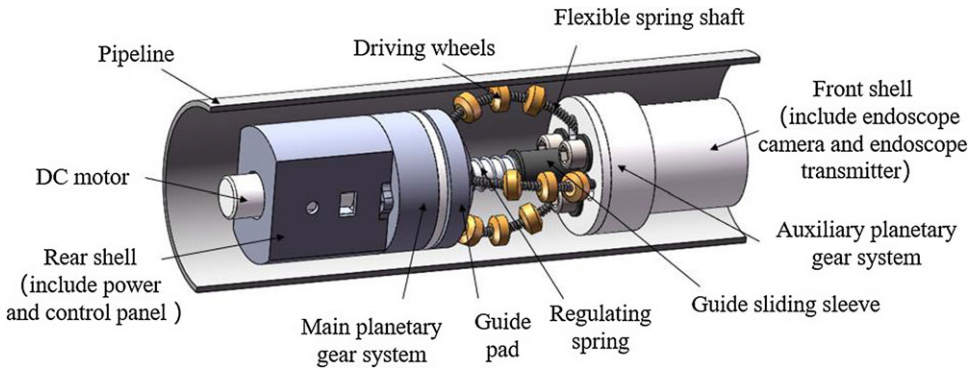


Figure 2. Model of in-pipe inspection robot (IPIR).

① The pipeline structure is complicated, and there are a large number of horizontal, inclined, and vertical pipelines, which puts forward requirements on pipeline adaptability and movement flexibility of the robot.

② Usually, the distance of the pipeline is long, and the inner wall of the pipeline has more resistance, which puts forward requirements on the power and endurance of the robot.

③ There are multi-diameter pipes and variable diameter nozzles in the pipeline, which puts forward requirements on the size adaptability of the robot.

④ The damages such as impurities, corrosion, and cracks on the inner wall of the pipeline are different, which puts forward requirements for robot detection scheme, technology selection, monitoring, and analysis quality.

In order to meet the above requirements and synthesize the advantages and disadvantages of various kinds of pipeline robots, this paper established a screw-driven IPIR, whose marching principle is based on screw drive. The threaded member rotates under the drive of torque. Due to the existence of the helix angle, the member has an axial component force, and under the action of this force, the threaded member can achieve helical advancement. Therefore, if the driving wheels are arranged in a spiral shape to form a certain helix angle, the robot can travel in a spiral shape.

In order to ensure the smooth running of the robot and easy control of the movement, a motor is used to drive, that is, one degree of freedom. The robot distributes three sets of driving wheels evenly at 120° and transmits power to them through mechanical structure. Under the action of compression nut, they stick to the inner wall of the pipe and overcome the frictional force.

The structure and transmission principle of the screw-driven robot may be depicted as in Figs. 2 and 3. The main structural components of the robot include DC motor, coupling, spline shaft, main planetary gear system, auxiliary planetary gear system, cardan joint, guide pad, flexible spring shaft, driving wheels, regulating spring, spherical plain bearing, guide sliding sleeve, front shell, rear shell, etc. Among them, the main planetary gear mechanism includes a box, a sun gear, three planetary gears, an internal gear, and a planetary carrier. The sun gear is fixed on the spline shaft, and the internal gear is fixed in the box. The robot model is divided into three parts: front, central, and back. The front end is equipped with an endoscope camera and endoscope transmitter, the back end is equipped with a power supply and control panel, and the central part is a spiral traveling device.

The transmission principle is to transmit the power of the back motor to the central traveling mechanism, driving the robot to move forward as a whole. Its specific transmission principle is as follows: The DC motor is fixed on the robot body, and the output shaft is connected with the spline shaft by coupling to transfer power. The main planetary gear system transmits power through the sun gear to drive the planet gear for rotation and revolution within the internal gear. The flexible spring shaft is interference connected with the planet gear through the universal joint and rotates and revolution with the planet gear. The driving wheels are firmly connected with the flexible spring shaft and rotate with the flexible

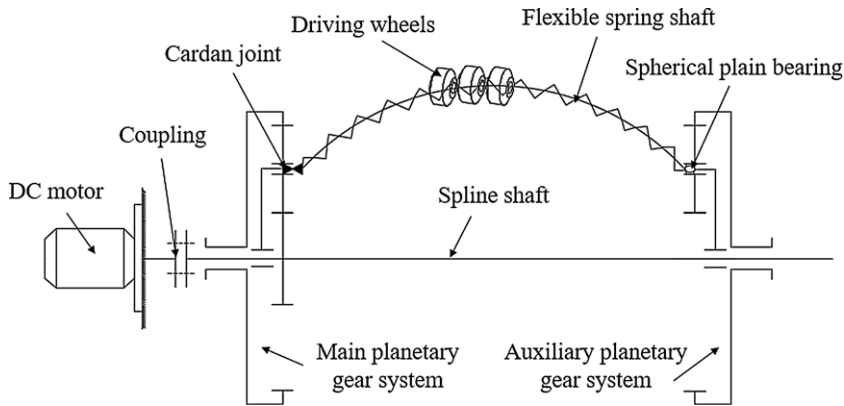


Figure 3. Transmission principle of in-pipe inspection robot (IPIR).

spring shaft under the driving force. The driving wheel adheres to the inner wall of the pipeline, driving the robot to spiral forward along the inner wall of the pipeline.

Significantly, in order to keep the transmission power stable, auxiliary planetary gear system mechanism away from the motor is not complete, there is no sun gear inside. The flexible spring shaft rotates with input power only on one side. What's more, the two planetary gear system mechanisms do not correspond along the axis, there is a staggered angle by guide sliding sleeve, so as to achieve the axis of the driving wheel and the axis of the pipeline to produce a spiral angle, to achieve the robot spiral forward.

Using this spiral structure composed of flexible spring shaft, the robot moves close to the inner wall of the pipeline. Therefore, it can be applied to horizontal, inclined, and vertical pipelines. The above-mentioned application requirement ① is met.

At present, pipeline robots often use cable power supply, and need to be equipped with corresponding lengths of cables as the robot advances. Although this method can ensure the power supply of the robot, it greatly limits the flexibility of the robot and also causes waste of cables. Taking into account the complicated situation of pipelines and the rapid development of the battery industry, the robot adopts a cableless power supply method and is equipped with lithium batteries (with a capacity of 7500mAh), which can effectively store electricity, and at the same time, it has a small weight and small volume, which is suitable for robots to travel long distances. The rated power of the robot motor is 15W, and considering the energy discharge loss efficiency of 80%, the robot can operate continuously for 4.8h. Therefore, the above-mentioned application requirement ② is met.

2.2. Adaptability and softness of robot to variation of pipe diameter

In general, pipe diameter changes often occur during pipe design and use, so the robot must be able to adapt to pipe diameter changes within a certain range. The adaptability of diameter adopts the bionic principle, and the dimension deformation principle is similar to the inchworm crawling. The inchworm propels itself by repetitive contraction and expansion movements. The adaptability and softness of the robot to the change of pipe diameter depends on the bending deformation of the flexible shaft. The flexible spring shaft is composed of high-strength steel wire through bi-directional multi-layer winding, which has the characteristics of smooth, flexible, high elasticity, and low vibration and can withstand large static torsional moment of destruction, while the strength can also meet the requirements of use.

Figure 4 shows the schematic diagram of the functional principle of adaptability of robot. The two ends of the flexible spring shaft are respectively fixed in the main and auxiliary planetary gear. The main planetary gear system is axially fixed to the robot body, while the auxiliary planetary gear system can slide on the spline shaft. Under the spring force and the gland nut, the flexible spring shaft has different

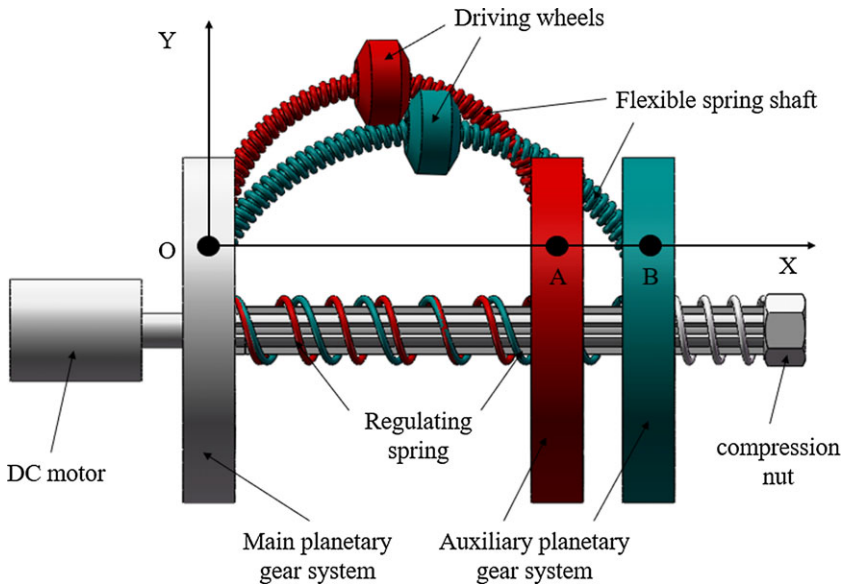


Figure 4. Schematic diagram of in-pipe diameter adaptive module.

degrees of bending deformation. When the nut compression force is small, the flexible spring shaft appears OB shape, and the diameter of the cylindrical surface formed by the driving wheels is small, which is suitable for small-diameter pipeline. When the nut compression force is large, the flexible spring shaft shows OA shape, and the diameter of the cylinder formed by the driving wheels is large, which is suitable for large-diameter pipe.

When the robot is in use, the compression nut is pre-adjusted to the appropriate position according to the range of pipeline diameter size. When the robot faces different pipeline diameters, it can rely on spring elastic deformation to adapt to pipeline diameter changes. The size parameters of the key components (such as flexible spring shaft/spline shaft) of the robot are different, and the suitable pipe diameter range is also different. It is necessary to determine the pipe diameter adaptation range through theoretical analysis and experimental testing and mark it on the spline shaft to facilitate pre-adjustment of the position of the compression nut. The theoretical analysis process is shown in the following text, and data modeling analysis is conducted on the stress and deformation of key components of the robot. Based on the result (L) of theoretical analysis, an interval ($L - \Delta_L, L + \Delta_L$) is set on the spline shaft for experimental testing, and the deformation status and usage effect of the robot are compared. Next, the set point is continuously optimized through the dichotomy method to adjust the appropriate position of the compression nut. In fact, this is a continuous debugging process, so the specific experimental debugging process is omitted. The debugging experimental results are shown in Chapter 4.3.

It should be noted that Fig. 4 is only a schematic diagram of the deformation principle. The flexible spring shaft and spline shaft inside the robot are not in the same plane, but there is a staggered angle in Fig. 5(a). Therefore, the influence of the staggered Angle should be considered first when analyzing the force of the flexible shaft spring. A spatial coordinate system is established to decompose the force F at the end of the flexible spring shaft into the force F_{AB} along the flexible spring shaft plane AB and the force F_{CD} perpendicular to the plane CD, the staggered Angle between them is α .

$$\begin{cases} F_{AB} = F \cos \alpha \\ F_{CD} = F \sin \alpha \end{cases} \quad (1)$$

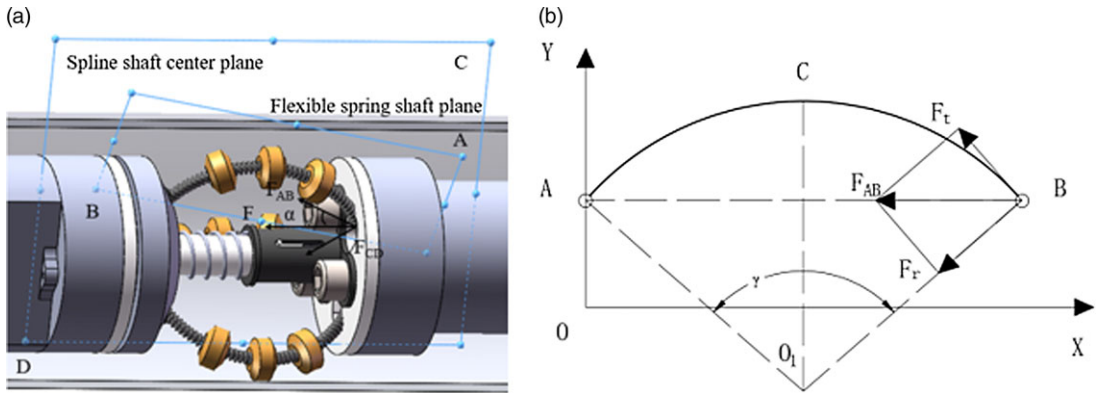


Figure 5. (a) Force analysis of flexible spring shaft. (b) Force equivalent model of flexible spring shaft.

F is influenced by the spring elasticity

$$F = k_1x_1 - k_2x_2 \tag{2}$$

where k_1, x_1, k_2, x_2 is the elastic coefficient and deformation of the two springs, respectively.

Along the flexible spring shaft plane AB, due to the particularity of the spring shaft, the shearing deformation and the cantilever length changing with the load should be considered, so the flexible shaft spring and the flexible shaft are analyzed separately. The flexible spring shaft is equivalent to an equivalent cantilever beam with one end fixed and the other end free. The analysis process can be carried out according to the equivalent cantilever beam, and the influence of shear deformation and cantilever length with load change is considered.

Figure 5(b) shows the force equivalent model diagram of the spring flexible shaft. Rod AB is elastomer and flexible shaft equivalent straight rod. The bar is fixed at A and subjected to axial force F_t and radial force F_r at B. Since both F_t and F_r have obvious effects on rod AB, axial load and shear deformation are analyzed separately for the convenience of analysis. Ignoring the influence of cutting deformation, the following differential equation holds:

$$\frac{d^2x}{dt^2} + \frac{F_t}{B}x = -\frac{F_t F_r (H - t)}{B F_t} \tag{3}$$

where H is the original effective length of the flexible spring shaft and B is the bending stiffness of the equivalent cantilever beam.

The radial deformation of the loaded end of the spring can be obtained by adding boundary conditions to solve the equation:

$$\Delta = \lambda \cdot \xi \tag{4}$$

where $\lambda = \frac{F_r H^3}{3B}, \xi = \frac{3(\tan u - u)}{u^3} (u = H \sqrt{\frac{F_{AB}}{B}})$

λ corresponds to the fact that only the radial load F_r acts on the loaded end of the spring, and the radial deformation during cutting deformation is not considered. ξ corresponds to the influence of axial load F_t on radial deformation Δ .

Under the action of radial load, the spring shaft has radial deformation considering cutting deformation:

$$\Delta = \frac{F_r H^3}{3B} + \frac{F_r H^3}{S} = \lambda \cdot \chi \tag{5}$$

where S is the shear stiffness of the equivalent cantilever beam, $\chi = 1 + \frac{3B}{H^2 S}$, χ is the influence of the shear deformation on the radial deformation.

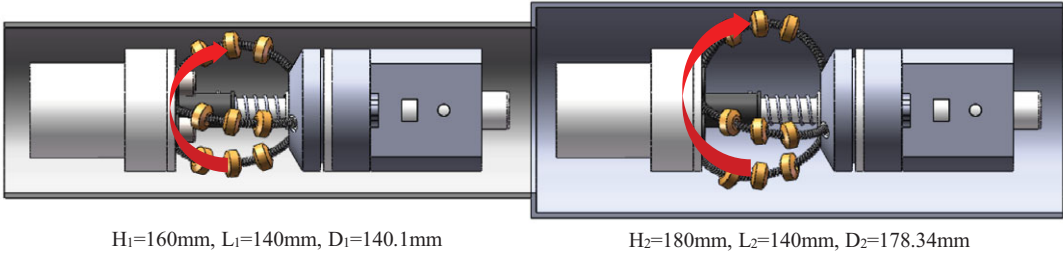


Figure 6. Robot adaptive to pipe diameter change.

Based on the above analysis, when the spring axis is subjected to both radial load F_r and axial load F_t , the deformation of the loaded end B is calculated as:

$$\Delta_B = \lambda \cdot \xi \chi \tag{6}$$

Ultimate load

$$F' = \frac{S}{2} \left[\sqrt{1 + \left(\frac{\pi}{H}\right)^2 \frac{B}{S}} - 1 \right] \tag{7}$$

The deformation of point C in the center of the flexible axis along the Y-axis is:

$$\Delta_C = \frac{H}{\gamma} - \frac{H - \Delta_B}{2 \tan \frac{\gamma}{2}} \tag{8}$$

Therefore, the adaptive pipe diameter of the robot is $D = 2(\Delta_C + C)$.

where C is a constant and the value is the radius of the rotation trajectory circle of the central axis of the planetary gear. It can be seen that under the condition that the material characteristics are determined, the adaptability of the robot to the pipe diameter is affected by the original length of the flexible spring shaft H , the radial force F_r , and the corresponding central angle γ . Therefore, the adaptive pipe diameter size can be changed by adjusting these parameters.

The preset position point of the compression nut can be determined by the theoretical analysis of the chord length AB, and the chord length formula shows:

$$L = 2R \sin \gamma = \frac{2(H - \Delta_B)}{\gamma} \sin \gamma \tag{9}$$

Figure 6 provides a simulation diagram that robots are used in different pipe diameters. In the figure, when the bending chord length L of the flexible spring shaft is equal, the longer the original length H of the flexible spring shaft, the larger the diameter of the robot, which is consistent with the theoretical analysis results mentioned earlier. At the same time, the adaptability range of the pipe diameter can also be changed by changing the degree of bending deformation of the three flexible spring shafts, which can be analyzed through experiments. Therefore, it meets the above application requirements ③.

2.3. Robot real-time detection and control

At present, the detection methods commonly used for pipeline robots at home and abroad are as follows: ultrasonic ranging detection [38], infrared thermal imaging detection [39], and camera vision detection [40, 41]. Among them, ultrasonic ranging detection method uses different acoustic reflection to detect pipeline defects, and infrared thermal imaging method uses different heat exchange temperature to detect. However, these methods are not as intuitive as the camera visual detection method. The camera visual detection is able to visually display the internal state of the pipeline by installing a CCD camera for image acquisition and analysis.

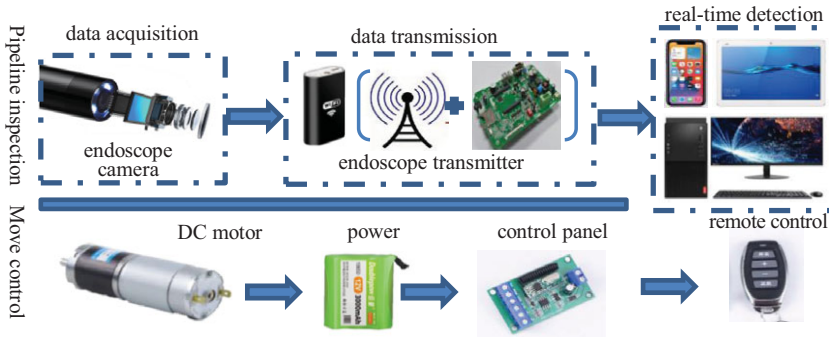


Figure 7. Pipeline detection and movement control.

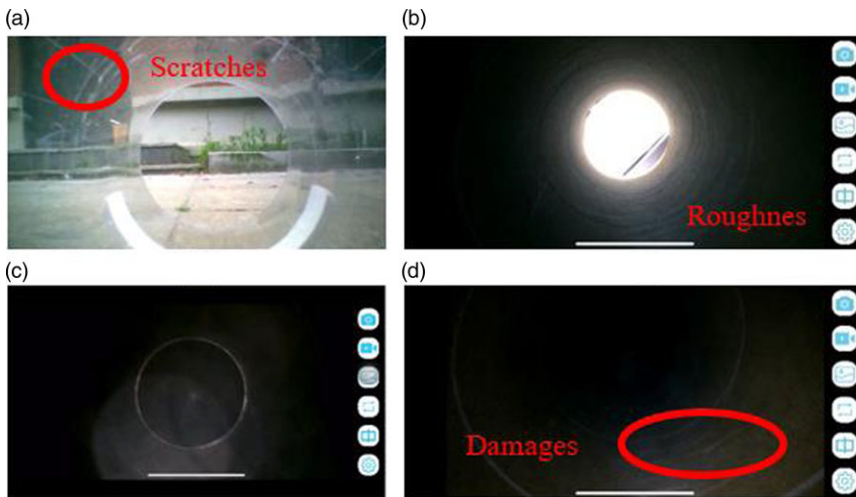


Figure 8. Test example, (a) light state of acrylic pipeline, (b) light state of paper tube, (c) dark state of acrylic pipeline, (d) dark state of paper tube.

The real-time detection of the robot adopts the camera visual detection method. A high-definition endoscope camera (5MP) is installed in the center of the front shell of the robot to conduct real-time acquisition of the internal environment and state data of the pipeline, and data transmission is carried out through the schematic diagram shown in Fig. 7 to realize real-time detection.

The principle of detection is as follows: the endoscope camera collects data inside the pipeline, and the monitoring information is transmitted to the upper computer software through the Wi-Fi wireless communication module inside the endoscope transmitter. The software can store the data collected each time and establish a database. Through the above steps, information collection and transmission can be completed. Finally, the upper computer software can be installed on wireless network devices such as mobile phones, tablets, and computers to check the inner wall of the pipeline.

Figure 8 is an experimental diagram of the robot detection, which involves using mobile phones to monitor the inner wall of pipelines in two materials: acrylic and paper tube, and in two states of light and darkness. From the figure, it is clear to see the scratches, damages, and roughness of the pipeline inside. And the robot monitoring camera can be flexibly replaced, and high-precision pipeline detection can be carried out by replacing a higher-definition camera or different types of lenses (such as fisheye camera). Therefore, it meets the above application requirements ④.

The principle of robot motion control is as follows: the power of the robot comes from the planetary DC deceleration motor, equipped with lithium battery to provide energy, through the control board and

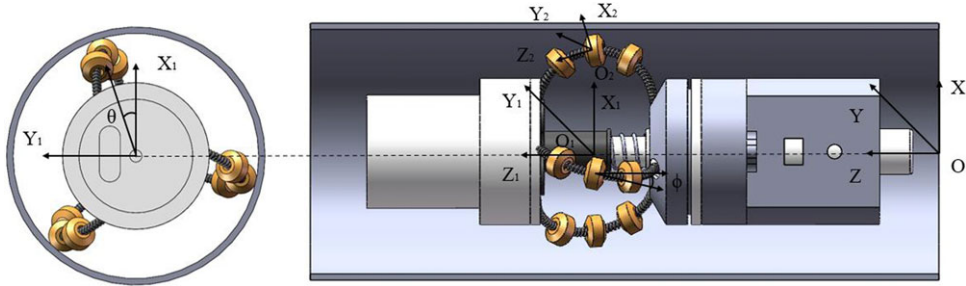


Figure 9. Robot of kinematics model.

wireless remote control can realize the robot remote control, to achieve forward, backward and stop and other actions.

3. Motion mechanism of IPIR

3.1. Kinematics of robot

As shown in Fig. 9, {O} is the global coordinate system. O₁ is the intersection point between the section formed by the middle drive wheel on the three flexible spring shafts and the robot's rotation axis, its coordinates are (0,0,z)^T. {O₁} is the moving coordinate system on the robot. The X₁Y₁ plane of coordinate system O₁ is parallel to the XY plane of coordinate system O. The robot rotates around the Z axis at an angular velocity $\dot{\theta}$. The included angle between the driving wheel and X₁ axis is θ . {O₂} is the moving coordinate system on the driving wheels. The angular velocity of the driving wheel about the X₁ axis is $\dot{\alpha}$. The spiral angle between the driving wheel surface and the radial section of the pipe is α . The radius of the driving wheel is r_s, the contact point between the driving wheel and the inner wall of the pipe is S, and its coordinates in coordinate system O₂ are (r_s,0,0)^T. The homogeneous change matrix of each coordinate system and the pose matrix of contact point S in the global coordinate system {O} are as follows:

$${}^0T_1 = \begin{bmatrix} \cos \theta & -\sin \theta & 0 & 0 \\ \sin \theta & \cos \theta & 0 & 0 \\ 0 & 0 & 1 & z \\ 0 & 0 & 0 & 1 \end{bmatrix} \tag{10}$$

$${}^1T_2 = \begin{bmatrix} 1 & 0 & 0 & \frac{D}{2} - r_s \\ 0 & \cos \alpha & -\sin \alpha & 0 \\ 0 & \sin \alpha & \cos \alpha & 0 \\ 0 & 0 & 0 & 1 \end{bmatrix} \tag{11}$$

$$[S \ 1]^T = {}^0T_1 {}^1T_2 [r_s \ 0 \ 0 \ 1]^T \tag{12}$$

Thus, the point S in the {O} coordinate system can be expressed as:

$$S = \begin{bmatrix} \frac{D}{2} \cos \theta \\ \frac{D}{2} \sin \theta \\ z \end{bmatrix} \tag{13}$$

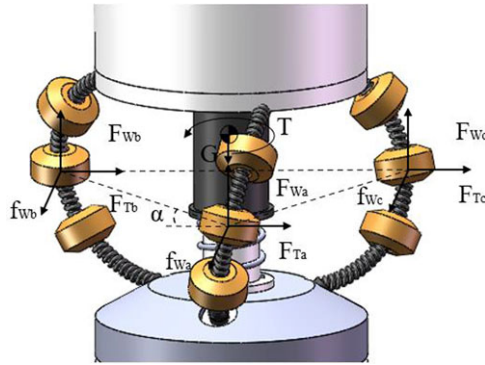


Figure 10. Forces and torque when the robot climbs up in a vertical pipe.

Taking the derivative of time, the velocity expression of the contact point S between the driving wheel and the pipe wall can be written as follows:

$$\dot{S} = \begin{bmatrix} -\frac{D}{2} \sin \theta \dot{\theta} \\ \frac{D}{2} \cos \theta \dot{\theta} \\ \dot{z} \end{bmatrix} \tag{14}$$

The Z_2 direction vector is as follows:

$$e_{Z_2} = \begin{bmatrix} \sin \alpha \sin \theta \\ -\sin \alpha \cos \theta \\ \cos \alpha \end{bmatrix} \tag{15}$$

No axial slide of the drive wheel is assumed, that is, the projection of the speed \dot{S} on the Z_2 axis is zero.

$$\dot{S} \cdot e_{Z_2} = 0 \tag{16}$$

The \dot{z} is calculated as:

$$\dot{z} = \frac{D}{2} \tan \alpha \dot{\theta} \tag{17}$$

It can be seen that when the spiral angle α is fixed, the running speed of the screw-driven in-pipe inspection robot is only related to the rotation speed of the driving wheel. By changing the size of the spiral angle α , the speed of the screw-driven robot can be changed, and the running posture and stability of the screw in-pipe robot will be affected.

3.2. Dynamics of robot

The robot moves through this screw mode, the axis of the driving wheel is not parallel to the axis of the pipe, the driving wheel is always close to the pipe wall under the action of the spring force and moves under the action of the rotating torque of the external motor. Therefore, the robot can travel in a straight pipe, regardless of whether the pipe is horizontal or inclined or vertical.

Figure 10 shows the force analysis diagram of the working section of the robot. The center of mass of the robot is located at the central point, and the three groups of driving wheels are respectively subjected to F_{wa} , F_{wb} , and F_{wc} from the pipe wall; the friction forces between the driving wheels and the pipe wall are respectively f_a , f_b , and f_c . The robot moves under the driving force of F_{Ta} , F_{Tb} , and F_{Tc} . In ideal condition, $F_{wa} = F_{wb} = F_{wc}$, $F_{Ta} = F_{Tb} = F_{Tc} = \frac{T}{3R}$, $f_a = f_b = f_c$. As the friction force f_a , f_b , and f_c are

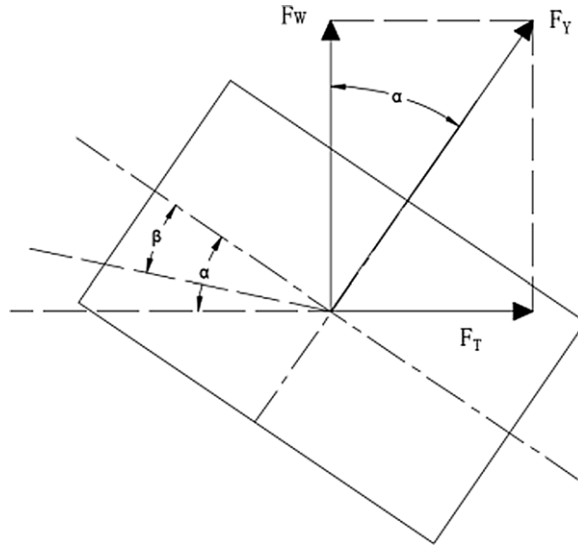


Figure 11. Forces of driving wheel.

rolling friction force, the friction coefficient is small, so the influence of friction force is ignored. Take one of the driving wheels and analyze its load and driving force as shown in Fig. 11.

The conditions that the spiral pipe robot can move forward in the pipe are as follows: ① The resultant force of the driving force F_T and the load force F_w in the rolling direction of the driving wheel is 0; ② the resultant force of driving force F_T and load force F_w is F_Y , and the slip angle β generated by F_Y is not greater than spiral angle α ; ③ the driving wheel can provide enough friction, and no slippage occurs. Hence:

$$F_T \cos \alpha = F_w \sin \alpha \tag{18}$$

$$F_T \sin \alpha + F_w \cos \alpha = W(\beta) \tag{19}$$

$$\beta \leq \alpha \tag{20}$$

The maximum tractive force produced by the system is the tractive force when $\beta = \alpha$:

$$F_w = F_Y(\beta) \cos \alpha \quad \alpha = \beta \tag{21}$$

Relation between force F_Y on the driving wheel and lateral slip rate \varnothing :

$$F_Y = \begin{cases} \left(1 - \frac{1}{4\varnothing}\right) \mu N & \varnothing > 1/2 \\ \varnothing \mu N & \varnothing \leq 1/2 \end{cases} \tag{22}$$

where $\varnothing = \frac{K_y \tan \beta}{uN}$, K_y is the lateral stiffness of the wheel, and μ is the adhesion coefficient.

Substitute:

$$F_w(\alpha) = \begin{cases} \left(1 - \frac{\mu N}{4K_y} \cot \alpha\right) \mu N \cos \alpha & \frac{K_y \tan \alpha}{uN} > 1/2 \\ K_y \sin \alpha & \frac{K_y \tan \alpha}{uN} \leq 1/2 \end{cases} \tag{23}$$

The relation between tractive force and Angle α can be obtained after substitution, and the tractive force increases with the increase of spiral angle α . When the spiral angle α increases to a certain value, the traction force decreases as the spiral angle α continues to increase. When the driving wheel is perpendicular to the pipeline axis, the traction force decreases to 0. Therefore, the traction force can be

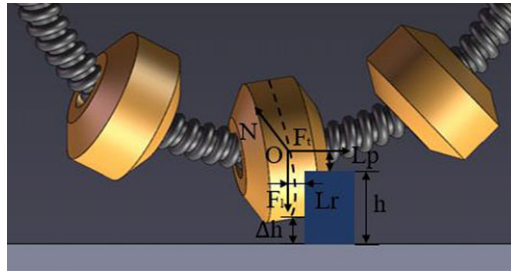


Figure 12. Analysis on obstacle capability of driving wheel.

changed by adjusting the spiral angle. A major feature of steel wire flexible shafts is their strong flexibility, which allows for elastic deformation in multiple planes, resulting in slightly different spiral angles at different driving wheel positions. When facing complex operating conditions, the robot can obtain maximum traction force through the elastic deformation of the flexible shaft.

3.3. Analysis on obstacle capability

When the robot travels along the pipeline, the inner diameter of the pipeline is not invariable. On the contrary, the pipeline is often welded by different pipelines, which leads to some bumps or grooves in the pipeline that are difficult to eliminate. Whether the robot can overcome such obstacles is also an important part to test the stability of the robot.

Under the elastic support of the flexible spring shaft, the driving wheels are pressed against the inner wall of the pipeline to generate pressure, and the motor torque is converted into the axial driving force by the normal static friction force. The static equilibrium relation satisfies the following relation:

$$F = \frac{2Mi_H}{D \tan \alpha} \tag{24}$$

$$F = nf_n \cos \alpha \tag{25}$$

where F is the axial traction force of the robot, M is the output torque of the DC motor, i_H is the transmission ratio, n is the number of wire flexible shafts, f_n is the normal friction force, and α is the spiral angle.

It is assumed that there are n flexible spring shafts distributed inside the screw-driven in-pipe robot. Taking the driving wheel on one of the flexible spring shafts as an example, the force analysis as shown in the Fig. 12 is carried out to establish the model of robot obstacle capability. Among them, the blue identification block marks the boss, whose height is h , and the vertical lifting height between the robot driving wheel and the inner wall of the pipeline is Δh . When the driving wheel is in contact with the obstacle, the contact edge point has a supporting force N on the driving wheel. In addition, the driving wheel is also subjected to the traction force F_t needed to cross obstacles, and the elastic force F_l of the flexible spring shaft under compression deformation.

If the robot can successfully cross the obstacle, the following conditions need to be met:

- ① The kinetic moment of the driving wheel is greater than the resistance moment.

The robot traverses the obstacle slowly, which can be considered as a quasi-static process. Therefore, based on the quasi-static equilibrium point of the contact point of the driving wheel edge, the relationship between kinetic moment M_p and resistance moment M_r is as follows:

$$M_p = F_t L_p \geq M_r = F_l L_r \tag{26}$$

F_t, L_p, F_l, L_r is respectively:

$$F_t = \frac{Mi_H}{n(\frac{D}{2} - h) \tan \alpha} \tag{27}$$

$$L_p = r_s + \Delta h - h \tag{28}$$

$$F_l = F_0 + k\Delta h \tag{29}$$

$$L_r = \sin \alpha \sqrt{r_s^2 - (r_s + \Delta h - h)^2} \tag{30}$$

where k is the elastic stiffness coefficient of the flexible spring shaft, and F_0 is the elastic preload.

Therefore, the minimum torque is as follows:

$$M_{min} = \frac{n(F_0 + k\Delta h)(\frac{D}{2} - h) \tan \alpha \sin \alpha \sqrt{r_s^2 - (r_s + \Delta h - h)^2}}{(r_s + \Delta h - h) i_H} \tag{31}$$

② The normal static friction force f_n of the driving wheel does not exceed the maximum normal static friction force $f_n \max$.

$$f_n = \frac{Mi_H}{n(\frac{D}{2} - h) \cos \alpha} \leq f_n \max = \mu N \tag{32}$$

Therefore, the maximum torque is:

$$M_{max} = \frac{n\mu N(\frac{D}{2} - h) \cos \alpha}{i_H} \tag{33}$$

When the robot’s driving wheel crosses obstacles, the maximum motor output torque that can be provided while ensuring that the driving wheel does not slip and the motor is not overloaded is:

$$M = \min(M_{min}, M_{max}) \tag{34}$$

4. Experiment and results

4.1. Horizontal, vertical, and oblique travel

The prototype and experimental model of the screw-driven in-pipe inspection robot(IPIR) are shown in Fig. 13, and the specific parameters of the prototype are shown in Table II. The robot prototype can be divided into three parts. The head is equipped with an endoscope camera to realize real-time monitoring of the state in the pipeline. The tail is the power source and control module of the prototype, which provides and transmits power to the robot. The central part is a walking device, which not only realizes the spiral advance along the pipeline but also can adjust the deformation degree to realize the self-adaptation of pipe diameter size.

To facilitate the observation of the robot’s moving process, a transparent acrylic round tube with an inner diameter of 129 mm and a length of 700 mm is selected to build the robot’s moving experiment model. The tube is installed horizontally, vertically, or obliquely (with a slope of 1:6) on the bracket, and the robot is put into the tube from one end. The motor is started with rotating forward to observe the progress of the robot’s forward, and then, the motor is started with reverse to observe the progress of the robot’s backward, and photos are taken every 10 s.

The experimental results of horizontal/vertical/oblique directions are shown in Figs. 14, 15, 16. The three modes of movement all involve the process of forward and backward movement. Among them, it should be noted that in order to facilitate the observation of the motion of the three flexible spring shafts of the robot, a black insulation layer is wrapped around the driving wheel on one of the flexible spring shafts.

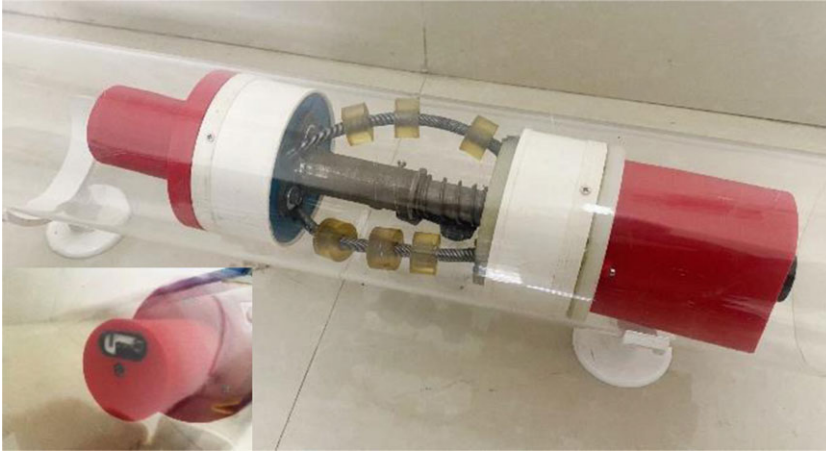


Figure 13. Prototype of screw-driven in-pipe inspection robot (IPIR).

In horizontal working conditions, the power is output to the three uniform flexible spring shafts after the motor starts. The flexible shaft is subjected to torsion deformation and driving wheels are firmly pressed on the inner wall of the pipeline. Under the connection of the guide sliding sleeve component, the flexible shaft is staggered between the main and auxiliary planetary gear system, resulting in a 15° spiral angle between the driving wheel axis of the prototype model and the pipeline axis. Therefore, when the driving wheel rotates on the inner wall of the pipeline, it can drive the robot to move forward or backward along the axis direction. Due to the horizontal installation of the pipeline, the robot's forward and backward processes are subjected to the same force, and its motion speed and stability are also consistent.

By replacing the pipeline support, the operating condition with a slope of 1:6 is established. The robot can also move forward and backward in the pipe with a certain oblique Angle, and the speed is basically the same. However, in the process of backward, the robot's operation stability is poor. Due to the influence of gravity, partial instability of the flexible shaft can be observed in Fig. 15. This is due to the flexibility of the flexible spring shaft, which increases the spiral angle through deformation in order to obtain greater driving force.

Place the pipe vertically to establish the vertical condition. The experimental results show that the robot can move both downwards and upwards along a vertical pipeline, but the motion velocity of the two directions is quite different. When the robot is vertically down, the robot travels faster due to positive work done by gravity, while when it is vertically up, the robot travels slower due to negative work done by gravity.

Moreover, the stability of the robot is also poor, and the instability of the flexible shaft can be seen in many places. This is affected by the precision of robot prototype model making. The robot travels in the pipeline relying on the support of three evenly distributed flexible spring shafts. Theoretically, the three flexible shafts have the same length. In fact, the installation accuracy in the length direction is difficult to guarantee during the connection process, resulting in errors between the three flexible shafts in the robot model, and the degree of deformation is not completely consistent. In the aforementioned 3.2, the plane formed by the central driving wheel on the flexible shaft is not completely parallel to the pipe section, but has a certain inclination angle. When the robot moves vertically, the moving resistance increases, the deformation of the flexible spring shaft increases, and the instability of the movement process is more obvious. Therefore, during the production and installation of robots, it is necessary to improve the installation accuracy, so as to alleviate the instability of motion.

Table II. *Parameters of the robot prototype.*

Parameter	Numerical
Axial length	400 mm
Weight	3.5 kg
Radial dimension of Shell	116 mm
Length of flexible spring shaft	160 mm
Minimum-maximum outside diameter	120–138 mm
Spiral angle α	15°
Rated torque	28 kgf.cm
Speed	58 r/min

**Figure 14.** *Horizontal process.*

4.2. Obstacle crossing

The aforementioned analysis shows that in order to increase the scope of application of the robot, it is necessary to consider the robot's obstacle crossing ability. According to the principle of robot movement, the prerequisite for a robot to overcome obstacles is to have the ability to adapt to different pipe diameters. The theoretical analysis of the robot's pipe diameter adaptability is conducted in Section 2.3, and experiments are designed in this section to verify the robot's adaptability to pipe diameters.

As shown in Fig. 17, the inner diameters of the three sections of the pipeline are 124, 131, and 138 mm, and they are sequentially connected to form a complete pipeline. The robot is placed vertically, the pipeline is inserted from one end, the motor is started, and records are made every 5 s.

The relative motion between the robot and the pipe can be observed in the Fig. 17. With the rotation of the motor, the power is transferred to the three flexible shafts, and the pipe moves down relative to the robot, making the pipe with a diameter of 138 mm pass through the robot first, and then, the motor continues to rotate. Under the elastic force of the flexible shaft, the diameter of the cylindrical surface formed by the three flexible shafts changes, so the pipe with a diameter of 131 and 124 mm can pass through the robot in turn. Therefore, the experiment shows that the robot has the ability to deal with the change of pipe diameter.

Next, the obstacle crossing ability is verified by experiment. A paper tube with an inner diameter of 123 mm is embedded inside the acrylic tube with an inner diameter of 129 mm to generate a 3 mm boss and build an experimental platform. After multiple experiments and recording every 5 s, it is found that the robot could enter from one end of the pipeline and successfully crossed the obstacle, and the process and details are shown in Fig. 18.

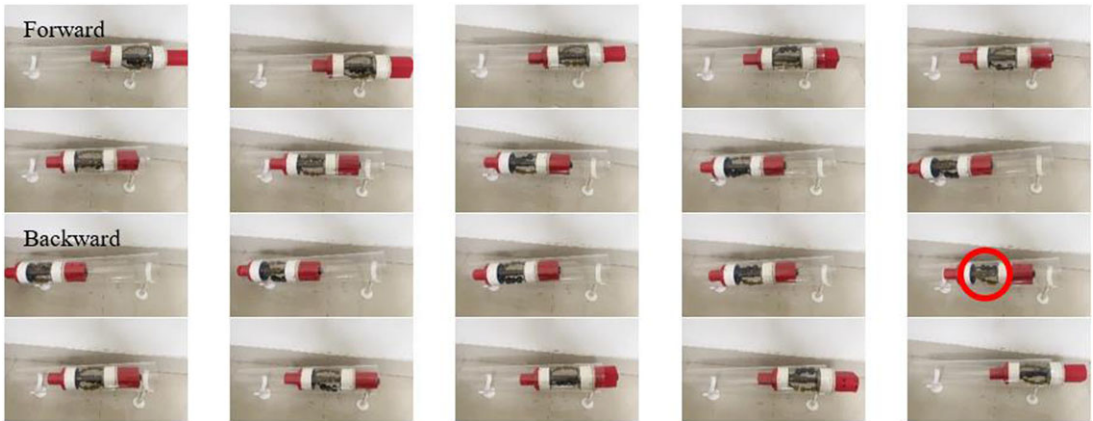


Figure 15. Oblique process.

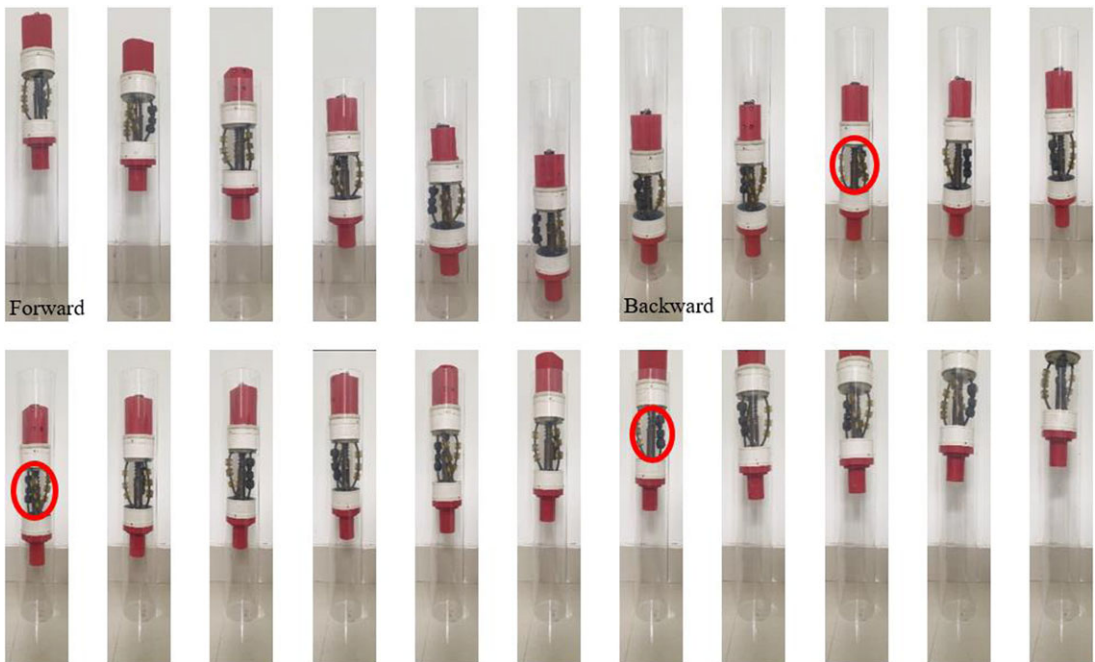


Figure 16. Vertical process.

At the beginning of the experiment, the flexible shaft and driving wheels of the robot are in the acrylic pipe. After starting the motor, driving wheels rotate with the flexible shaft, and driving wheels began to contact the paper pipe. Due to the influence of the annular boss, driving wheels could not directly pass through the pipe at first by a certain resistance, while the motor is still delivering torque continuously, which made the flexible shaft torsional deformation. Then, the spiral angle increase, and the power increase. Under the action of torque and friction, driving wheels gradually successfully pass through the 3 mm boss.

At the later stage of the experiment, as the motor continues to rotate, when driving wheels began to contact the acrylic pipeline, due to the elasticity of the flexible shaft and the deformable characteristics of the flexible shaft, it can realize that the driving wheel at different positions on the flexible shaft is in

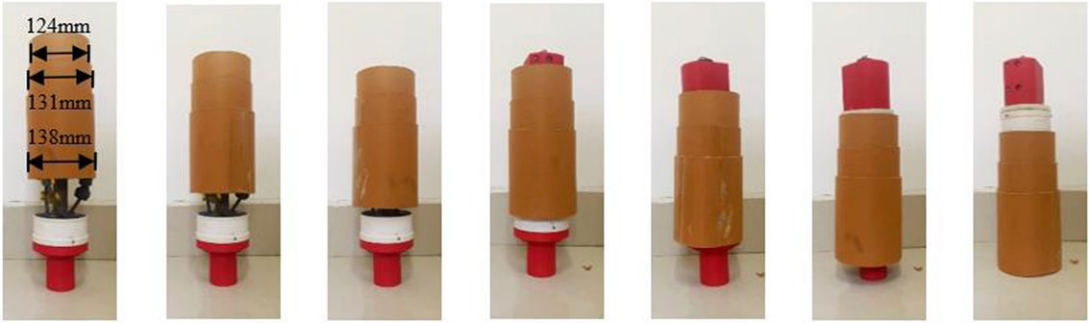


Figure 17. Different pipe diameters.



Figure 18. Obstacle crossing process.

close contact with the pipe, with enough friction to allow the robot move forward, so that the robot can pass through the pipe smoothly.

4.3. Performance analysis

The above analysis shows that the robot has the ability to operate under a variety of working conditions, but the performance of the robot's velocity and load capacity has not been reflected. The following is an experimental analysis of this. From the analysis of the robot's motion mechanism (chapter 3), it can be seen that the spiral angle formed by the flexible shaft is an important factor affecting the performance of the robot, and an experiment is designed for this.

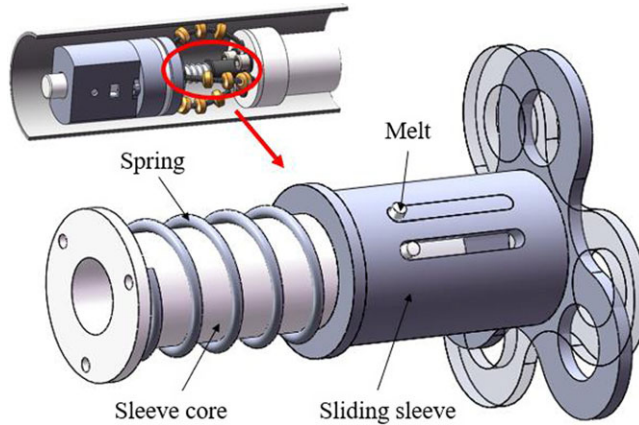


Figure 19. Guide sliding sleeve.

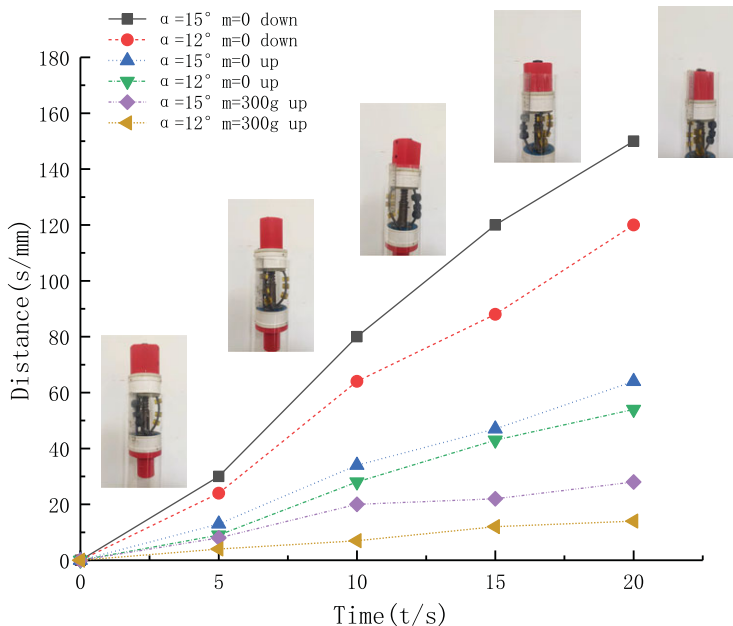


Figure 20. Distance-time relationship of the robot's running.

As shown in Fig. 19, the guide sliding mechanism is made up of sleeve core, sliding sleeve, spring, and melt. The sliding core is connected with the rear end of the robot, and the sliding sleeve is connected with the front end of the robot. There are two small holes on the upper part of the sliding sleeve, and the melt can be used to realize the two states shown in the figure, so that the flexible shaft spring presents two spiral angles α (12° , 15°). In order to analyze the load performance of the robot, a 300 g counterweight is hung at the end of the robot and compared with the state without counterweight. Since the robot moves in the vertical direction is the most difficult, this working condition is selected to conduct experiment, and the distance-time relationship of the robot's running is recorded, as shown in Fig. 20.

According to the distance-time diagram, it can be seen that there is a significant difference in the speed of the robot's vertical upward and downward movements. When the spiral angle is 15° and there is no counterweight, the average speed of the robot's vertically downward movement is 7.5 mm/s (The specific movement process is shown in the Fig. 20), while the average speed of the robot's vertical

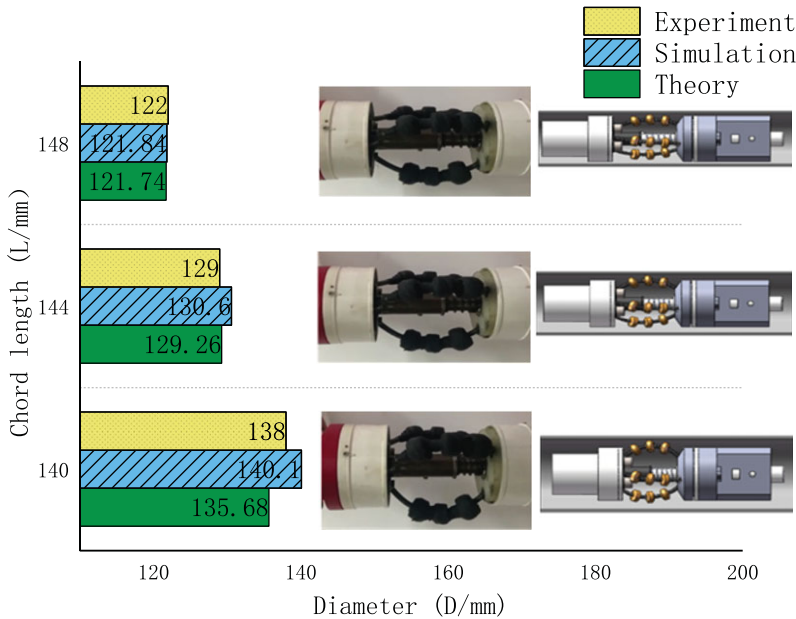


Figure 21. Chord length-diameter relationship of the robot.

upward movement is 3.2 mm/s, which is influenced by the work done by gravity. When the running direction and counterweight are consistent, the larger the spiral angle, the faster the robot runs, which is consistent with theoretical analysis. Through experiments, it can be seen that the robot can carry a 300g counterweight and move vertically upwards, but the motion speed is relatively low at 1.4 mm/s ($\alpha = 15^\circ$). When the spiral angle is 12° and the load is 300 g, the robot has low traction and is difficult to operate.

The robot’s adaptability to pipe diameter has been theoretically analyzed above. Now the theoretical, simulation, and experimental results are compared and analyzed. The relationship between bending chord length and diameter of the flexible shaft is shown in Fig. 21. From the figure, it can be seen that under the same initial length H of the flexible spring shaft, whether in theoretical analysis, numerical simulation, or experiment, the chord length becomes shorter and the diameter of the robot increases with the compression and deformation of the spring. When the compression chord length of the flexible spring shaft is large, the deviation of the robot diameter obtained by theoretical analysis, numerical simulation, and experiment is small, but when the spring chord length is compressed to 140 mm, the error of theoretical analysis and numerical simulation is large, with 1.68 and 1.52%, respectively. This is due to theoretical analysis and numerical simulation ignoring component interference, resulting in inconsistency with reality. Overall, certain data estimates can still be made through theory and simulation.

5. Conclusion and discussion

In this paper, a screw-driven in-pipe inspection robot has been proposed. Based on the deformation characteristics of flexible spring shaft and screw driving principle, the robot model is established, and the kinematics and dynamics analysis are carried out. In order to verify the motion behavior and expected results, a prototype model is built and tested under different conditions. The results show that:

1. The screw-driven robot has a new adapting mechanism. Wheel and tracked robots often use linkage deformation mechanisms to achieve a large range of diameter changes. Currently, screw-driven pipeline robots have not designed large deformation mechanisms, and only use simple spring support arms to achieve small range of robot diameter changes. However, the robot in the

article adopts a new variable diameter mechanism, which is a highlight of this article. The robot supports the flexible shaft through a planetary gear mechanism and utilizes the elastic deformation characteristics of the flexible spring shaft to achieve diameter variation. The prototype robot can pass through the pipe with a diameter of 120–138 mm and can change the adaptability range of the pipe diameter by changing the length H of the flexible shaft and increasing the radial force F_r , which is flexible and convenient.

2. The robot can achieve the traveling function of horizontal/vertical/oblique pipeline; among them, the forward and backward motion of robot in the horizontal and inclined directions is stable and the speed is basically the same, while the downward motion of robot is much faster than the upward motion in the vertical direction. However, the robot experiment did not include the analysis of pipeline pollution status, which needs to be strengthened in the future.
3. At the same time, the robot has certain ability to overcome obstacles and strong adaptability. It can pass smoothly through the 3 mm height of the circular steps.
4. Finally, the robot is equipped with an endoscope camera with 5MP, which can detect the transmission pipeline's internal environment state, to achieve the detection function.

In order to analyze the robot's travel performance, obstacle crossing performance, and load performance, multiple experimental environments (including three running directions: horizontal, vertical, and inclined, circular obstacles, and two materials of acrylic and paper tubes) have been established, and multiple sets of tests have been carried out. Although it has not been tested in a real pipeline, it can also effectively reflect part of the performance of the robot.

In the future, we will equip the robot with a vehicle-mounted manipulator to complete pipeline cleaning, spraying, welding, internal polishing, and other tasks, which has a good market application prospect. However, at present, the pipeline robot has not been analyzed in detail for the travel of curved pipeline, and it still needs to be improved.

Author contributions. All authors proposed the research and wrote the manuscript. Xuemei Liu instructed the research.

Financial support. None.

Competing interests. The authors declare that they have no competing interests.

Ethical approval. None.

References

- [1] P. Li, S. Ma, B. Li and Y. Wang, "Development of an Adaptive Mobile Robot for In-pipe Inspection Task," *2007 International Conference on Mechatronics and Automation*, **8** (2007).
- [2] H. Zhang, J. Zhang, R. Liu and G. Zong, "Realization of a service robot for cleaning spherical surfaces," *Int. J. Adv. Robot. Syst.* **2**(1), 53–58 (2008).
- [3] N. S. Roslin, A. Anuar, M. F. A. Jalal and K. S. M. Sahari, "A review: Hybrid locomotion of in-pipe inspection robot," *Proc. Eng.* **41**, 1456–1462 (2012).
- [4] A. Verma, A. Kaiwart, N. D. Dubey, F. Naseer and S. Pradhan, "A review on various types of in-pipe inspection robot," *Materials Today: Proceedings* **50**, 1425–1434 (2022).
- [5] M. Z. A. Rashid, M. F. M. Yakub, S. A. Z. bin Shaikh Salim, N. Mamat, S. M. S. M. Putra and S. A. Roslan, "Modeling of the in-pipe inspection robot: A comprehensive review," *Ocean Eng.* **203**, 107206 (2020).
- [6] A. J. Gh. Mills and R. Richardson, "Advances in the inspection of unpiggable pipelines," *Robotics* **6**(4), 36 (2017).
- [7] F. Zhou, X. Xu, H. Xu, Y. Chang, Q. Wang and J. Chen, "Implementation of a reconfigurable robot to achieve multimodal locomotion based on three rules of configuration," *Robotica* **38**(8), 1478–1494 (2020).
- [8] H. Jang, H. M. Kim, M. S. Lee, Y. H. Song, Y. Lee, W. R. Ryew and H. R. Choi, "Development of modularized in-pipe inspection robotic system: MRINSPECT VII+," *Robotica* **40**(5), 1361–1384 (2022).
- [9] Y. S. Kwon, B. Lee, I. C. Whang, W. K. Kim and B. J. Yi, "A flat pipeline inspection robot with two-wheel chains," *2011 IEEE International Conference on Robotics and Automation, Shanghai International Conference Center, Shanghai, China*, May 9–13 (2011) pp. 5141–5146.

- [10] W. Zhao, L. Zhang and J. Kim, "Design and analysis of independently adjustable large in-pipe robot for long-distance pipeline," *Appl. Sci.* **10**(10), 3637 (2020).
- [11] A. Zagler and F. Pfeifer, "'MORITZ': A Pipe Crawler for Tube Junctions," *Proceedings - IEEE International Conference on Robotics and Automation 3* (2003).
- [12] C. Choi, D. Chatzigeorgiou, R. Ben-Mansour and K. Youcef-Toumi, "Design and Analysis of Novel Friction Controlling Mechanism with Minimal Energy for In-pipe Robot Applications," *IEEE International Conference on Robotics & Automation IEEE* (2012) pp. 4118–4123.
- [13] M. G. Selvamuthu, R. Tadakuma, N. Fujiwara, K. Yoshida, M. Takagi, H. Hoshino, Y. Suzuri and H. Furukawa, "Development of soft inchworm robot with friction control of feet using double-network gel," *Adv. Robot. Int. J. Robot. Soc. Jpn.* **37**(6), 407–422 (2023).
- [14] M. M. Salvatore, A. Galloro, L. Muzzi, G. Pullano, P. Odry and G. Carbone, "Design of PEIS: A low-cost pipe inspector robot," *Robotics* **10**(2), 74 (2021). doi: [10.3390/robotics10020074](https://doi.org/10.3390/robotics10020074).
- [15] H. Zheng and E. Appleton, "Dynamic characteristics of a novel self-drive pipeline pig," *IEEE Trans. Robot.* **21**(5), 781–789 (2005).
- [16] J. T. Kahnemouei and M. Moallem, "A comprehensive review of in-pipe robots," *Ocean Eng.* **277**, 114260 (2023).
- [17] A. Gunatilake, P. Lasitha, K. Sarath, B. Stephen and V. Dammika, "Real-time 3D Profiling with RGB-D Mapping in Pipelines Using Stereo Camera Vision and Structured IR Laser Ring," *2019 14th IEEE Conference on Industrial Electronics and Applications (ICIEA) IEEE* (2019).
- [18] C. W. Ou, C. J. Chao, F. S. Chang, S. M. Wang, J. N. Lee, R. D. Hung, B. Chiu, K. Y. Cho and L. T. Hwang, "Design of an Adjustable Pipeline Inspection Robot with Three Belt Driven Mechanical Modules," *2017 IEEE International Conference on Mechatronics and Automation (ICMA) IEEE* (2017).
- [19] L. Xu, L. Zhang, J. Z. Zhao and K. Kim, "Cornering algorithm for a crawler in-pipe inspection robot," *Symmetry* **12**(12), 2016 (2020).
- [20] C. Yin, D. Tang and Z. Deng, "Development of Ray Nondestructive Detecting and Grinding Robot for Weld Seam in Pipe," *In: Robotics and Biomimetics IEEE* (2017).
- [21] S. U. Yang, H. M. Kim, J. S. Suh, Y. S. Choi, H. M. Mun, C. M. Park, H. Moon and H. R. Choi, "Novel Robot Mechanism Capable of 3D Differential Driving Inside Pipelines," *IEEE/RSJ International Conference on Intelligent Robots & Systems IEEE* (2014).
- [22] W. Jeon, J. Park, I. Kim, Y. K. Kang and H. Yang, "Development of High Mobility In-pipe Inspection Robot," *2011 IEEE/SICE International Symposium on System Integration (SII) IEEE* (2012).
- [23] Q. Xie, S. Liu and X. Ma, "Design of a novel inchworm in-pipe robot based on cam-linkage mechanism," *Adv. Mech. Eng.* **13**(9), 168781402110451 (2021).
- [24] Z. Zhang, L. H. Hu, X. H. Li and X. Y. Hu, "Motion analysis of screw drive in-pipe cleaning robot," *Proc. Inst. Mech. Eng. C J. Mech. Eng. Sci.* **236**(10), 5605–5617 (2022).
- [25] A. Kakogawa and S. Ma, "Stiffness design of springs for a screw drive in-pipe robot to pass through curved pipes and vertical straight pipes," *Adv. Robotics* **26**(3–4), 253–276 (2012).
- [26] C. Rusu and M. O. Tatar, "Adapting mechanisms for in-pipe inspection robots: A review," *Appl. Sci.* **12**(12), 6191 (2022). doi: [10.3390/app12126191](https://doi.org/10.3390/app12126191).
- [27] Q. Y. Liu, T. Ren and Y. H. Chen, "Characteristic analysis of a novel in-pipe driving robot," *Mechatronics* **23**(4), 419–428 (2013).
- [28] H. Yan, P. Zhao, C. Xiao, D. Zhang, S. Jiao, H. Pan and X. Wu, "Design and kinematic characteristic analysis of a spiral robot for oil and gas pipeline inspections," *Actuators* **12**(6), 240 (2023).
- [29] Y. Chen, Q. Liu and T. Ren, "A simple and novel helical drive in-pipe robot," *Robotica* **33**(4), 920–932 (2015).
- [30] P. Li, S. Ma, C. Lyu, X. Jiang and Y. Liu, "Energy-efficient control of a screw-drive pipe robot with consideration of actuator's characteristics," *Robot. Biomim.* **3**(1), 1–11 (2016).
- [31] T. Nishimura, A. Kakogawa and S. Ma, "Pathway Selection Mechanism of a Screw Drive In-pipe Robot in T-Branched," *Automation Science and Engineering (CASE), 2012 IEEE International Conference on IEEE* (2012).
- [32] A. Kakogawa and S. Ma, "Mobility of an In-pipe Robot with Screw Drive Mechanism Inside Curved Pipes," *IEEE International Conference on Robotics & Biomimetics IEEE* (2010).
- [33] E. Islas-García, M. Ceccarelli, R. Tapia-Herrera and C. R. Torres-SanMiguel, "Pipeline inspection tests using a biomimetic robot," *Biomimetics* **6**(1), 17 (2021).
- [34] B. Wang, K. Zhang, X. Ma and L. Jia, "A compliant leg design combining pantograph structure with leaf springs," *Robotica* **42**(2), 332–346 (2024).
- [35] E. N. Shahab, L. Bruzzone and P. Fanghella, "Porcospino, spined single-track mobile robot for inspection of narrow spaces," *Robotica* **41**(11), 3446–3462 (2023).
- [36] G. Chen, Z. H. Zhao, Z. Y. Wang, J. J. Tu and H. S. Hu, "Swimming modeling and performance optimization of a fish-inspired underwater vehicle (FIUV)," *Ocean Eng.* **271**, 113748 (2023).
- [37] G. Chen, X. Yang, Y. D. Xu, Y. W. Lu and H. S. Hu, "Neural network-based motion modeling and control of water-actuated soft robotic fish," *Smart Mater. Struct.* **32**(1), 015004 (2023).
- [38] S. Wickramanayake, K. Envelope, S. Kodagoda and L. Piyathilaka, "Ultrasonic thickness measuring in-pipe robot for real-time non-destructive evaluation of polymeric spray linings in drinking water pipe infrastructure," *Mechatronics* **88**, 102913 (2022).
- [39] H. Guan, T. Xiao, W. Luo, J. Gu, R. He and P. Xu, "Automatic fault diagnosis algorithm for hot water pipes based on infrared thermal images," *Build. Environ.* **218**, 109111 (2022).

- [40] A. Colvankar, S. Pawar and B. Patle, “In-pipe inspection robotic system for defect detection and identification using image processing,” *Mater. Today Proc.* **72**(3), 1735–1742 (2023).
- [41] K. Zhao, K. Yamaguchi and S. Onuki, “A preliminary experimental analysis of in-pipe image transmission based on visible light relay communication,” *Sensors (Basel, Switzerland)*. **19**(21), 4760 (2019).